Peer-reviewed version available at *Quant. Imaging Med. Surg.* **2018**, *8*, 770-780; doi:10.21037/qims.2018.09.03

Article

SPIO-loaded nanostructured lipid carriers as liver targeted molecular T2-Weighted MRI contrast agent

Xiu Liang Zhu [1,†], Chen Ying Lu [1,†], Zu Hua Wang [2,†], Ying Chen [1], Li Yong Jie [1], Qian Zhang [1], Wei Li [3], Yong Zhong Du [3,*], Ri Sheng Yu [1,*]

[1] Department of Radiology, The Second Affiliated Hospital, Zhejiang University School of Medicine, 88# Jiefang Road, Hangzhou 310009, China; E-Mails: zhuxiul@zju.edu.cn (X.L.Z.); luchenying@ zju.edu.cn (C.Y.L.); 2509048@ zju.edu.cn (Y.C.); jieliyong@ zju.edu.cn (L.Y.J.); 21618261@ zju.edu.cn (Q.Z.); risheng-yu@zju.edu.cn (R.S.Y.)

[2] College of Pharmaceutical Sciences, Guiyang College of Traditional Chinese Medicine, Guiyang 550002, China; E-Mails: wangrui551601@163.com (Z.H.W.)

[3] Institute of Pharmaceutics, College of Pharmaceutical Sciences, Zhejiang University, 866# Yuhangtang Road, Hangzhou 310058, China; E-Mails: lwei@zju.edu.cn (W.L.); duyongzhong@zju.edu.cn (Y.Z.D.)

† These authors contributed equally to this work

* Correspondence: risheng-yu@zju.edu.cn; Tel.: +86-13757118387; duyongzhong@zju.edu.cn; Tel.: +86-571-8820-8435

Abstract: The aim of this study was to develop a novel nanostructured lipid carriers (NLCs) with hepatocytes targeting as carriers for the magnetic resonance imaging (MRI) contrast agent (i.e., magnetic nanostructured lipid carriers, MNLCs), and to evaluate the targeting ability of the MNLCs with T2-weighted MRI both *in vitro* and *in vivo*. Here, the galactose-octadecylamine (Gal-ODA) conjugates were synthesized by chemical coupling reaction between lactose acid (LA) and octadecylamine (ODA). Then the superparamagnetic iron oxide (SPIO) loaded nanostructured lipid carrier (conjugated by Gal-ODA, Gal-NLC-SPIO) was prepared by emulsification-ultrasonic method using monoglyceride as lipid materials. The Gal-NLC-SPIO with a diameter of about 50 nm could specifically internalize into LO2 (human hepatic cell line) cells. *In vitro* MRI results also proved the specific targeting ability of Gal-NLC-SPIO to LO2 cells. The *in vivo* MR imaging experiments using an orthotopic intrahepatic xenograft tumor model further validated the hepatocytes targeted effect of Gal-NLC-SPIO. The results of this study suggested that Gal-NLC-SPIO can be used as a contrast agent to aid in the diagnosis of hepatic diseases.

Keywords: Superparamagnetic iron oxide; Magnetic resonance imaging; Solid lipid nanoparticles; Galactose; Liver-targeted

1. Introduction

Magnetic resonance imaging (MRI) is one of the most important and efficient non-invasive imaging tools in clinical diagnostics and biomedical research, especially for the early diagnosis of cancer [1,2]. In most cases of clinical application, magnetic resonance (MR) contrast agents (MRCAs) are utilized, not only to distinguish regions of diagnostic interest from background tissue but also to provide greater detail in images of abnormalities, revealing their exact sizes and characteristics once MRCAs have entered the specific tissues [3,4]. Specifically, MRCAs are employed to greatly alter the relaxation times of water molecules in their proximity, then increase tissue contrast on relaxation-weighted imaging sequences [5]. Hepatocyte-targeted MRCAs can provide useful information for evaluating hepatic diseases. For example, liver diseases such as hepatic tumor, hepatitis reduce the uptake of hepatocyte-targeted imaging agents into hepatocytes. Therefore, using hepatocyte-targeted contrast agents, hepatic diseases can be better evaluated non-invasively in

Peer-reviewed version available at Quant. Imaging Med. Surg. 2018, 8, 770-780; doi:10.21037/qims.2018.09.03

vivo [6]. There are two types of MRCAs: T1 and T2 MRCAs which affect the longitudinal and transverse relaxation times of water protons respectively. The typical examples of T1 MRCAs include gadolinium (Gd) complexes and manganese (Mn) oxide nanoparticles, also called positive MRCAs, produce hyperintense signal in T1-weighted images [7,8]. The classic examples of T2 MRCAs include superparamagnetic iron oxide nanoparticles (SPIO), also called negative MRCAs, produce hypointense signal in T2- and in T2*-weighted images [9,10]. The SPIO, because of their non-toxicity, great biocompatibility and suitable magnetic properties, have been intensively investigated as promising MRI probes. SPIO exhibit magnetic behavior only there is a magnetic field, so they are of great interest for applications in vivo and in vitro [9-11].

Drug targeted delivery system is largely founded on nanomedicine. These nanoparticles would be loaded with drug and targeted to specific parts of the body where there is solely designated tissue, thereby avoiding interaction with other unrelated tissue [12-17]. The goal of a targeted drug delivery system is to prolong, localize, target and have a protected drug interaction with the designated tissue, and the drug delivery systems are promising to minimize the side effects of cytotoxic drugs and to enhance their selective distribution [12,13]. There are two kinds of targeted drug delivery system: active targeted drug delivery, such as targeted to hepatic tumor or normal liver, and passive targeted drug delivery, such as engulfed by reticuloendothelial system (RES) [14-17]. Contrast agent targeted delivery system, like drug targeted delivery system, are gradually used for targeting diagnosis of disease [17].

In recent years, lipid based nanoparticles have been described as an amphiphilic nanocarrier for poorly water-soluble and lipophilic drugs. They have low toxicity due to their physiological lipid compositions [18-22]. Among lipid based nanoparticles, nanostructured lipid carriers (NLC) is a novel nanoparticle delivery system with complex architecture under development in recent years, which are composed of a solid lipid and an oil phase confers them higher stability and drug loading capacity as compared to solid lipid nanoparticles [20-22]. Because of its strong hydrophobic surface, after intravenous injection into the body, soon to be swallowed by RES, and into the liver and spleen by passive targeting [23,24].

On the other hand, NLC can be modified with ligand or antibody to achieve active targeting of tumor tissue [25-27]. Mammalian hepatocytes possess large numbers of high-affinity, cell-surface receptors (asialoglycoprotein receptor, ASGPR) that can bind asialoglycoproteins. It can specifically recognize ligands with terminal galactose residues. Each liver cell has more than 5 × 105 receptors in normal liver, but the number and function of the receptors was declined in hepatitis, cirrhosis, liver cancer and other liver diseases. Galactose (Gal) is a hepatocyte-specific ligand of ASGPR and the liver targeting group, which could induce and improve cell adhesion and the performance of liver extracellular matrix scaffold [26,27].

In this study, galactose-conjugated nanostructured lipid carriers (Gal-NLC) were prepared as a hepatocyte-targeting imaging probe to deliver magnetic SPIO nanoparticles (i.e., SPIO loaded Gal-NLC, Gal-NLC-SPIO), which could passively and actively target to liver due to active targeting modification with galactose in nano-carrier (Figure 1). Then we further investigated the targeting ability of nanoparticles to normal liver cells and hepatoma cells, and evaluated the diagnostic efficiency of hepatocellular carcinoma in vivo and in vitro.

Preprints (www.preprints.org) | NOT PEER-REVIEWED | Posted: 24 July 2018 doi:10.20944/preprints201807.0459.v1

Peer-reviewed version available at Quant. Imaging Med. Surg. 2018, 8, 770-780; doi:10.21037/qims.2018.09.03

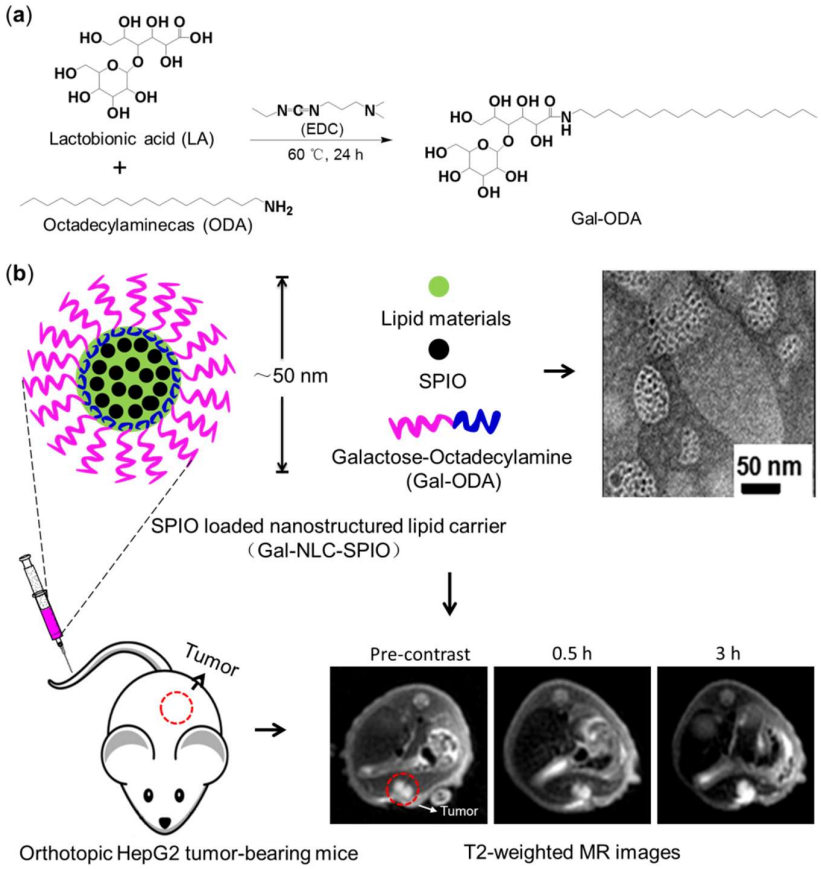

Figure 1. Schematic illustration of the Gal-NLC-SPIO nanoparticles. (a) Synthetic scheme of GAL-ODA; (b) Fabrication procedure of Gal-NLC-SPIO nanoparticles and further liver molecular MRI imaging.

2. Results

2.1. Synthesis and structure confirmation of Gal-ODA

Gal-ODA was synthesized by chemical reaction between the carboxyl group of LA and amino groups of ODA in the presence of water-soluble EDC-mediated condensation. The reaction scheme was shown in Scheme 1. The structure confirmation of Gal-ODA was determined via ^{1}H NMR spectra. Figure S1 showed the ^{1}H NMR spectrum of LA, ODA and Gal-ODA, respectively. The ^{1}H NMR chemical shift (about 12.5) of the proton of carboxyl group for LA was displaced to about 7.5, the chemical shift of the proton of amide group for Gal-ODA. These results indicated that Gal-ODA was synthesized successfully.

2.2 Preparation and physicochemical characteristics of MNLC

SPIO was purchased from Sigma-Aldrich Chemical (USA) and solvent diffusion method was utilized to prepare Gal-NLC-SPIO, NLC-SPIO and Gal-NLC-SPIO/PEG. Zetasizer and TEM were then employed to evaluate the size and morphology of MNLC. Particle diameter and zeta potential of Gal-NLC-SPIO, NLC-SPIO and Gal-NLC-SPIO/PEG were listed in Table S1. The results showed that three magnetic lipid nanoparticles are uniformly distributed (PI<0.3) and have negative charges, the particle sizes are similar. TEM photographs of Fe_3O_4, Gal-NLC-SPIO, NLC-SPIO and Gal-NLC-SPIO/PEG were showed in Figure 2. The photographs demonstrated the successfully entrapment of SPIO into Gal-NLC-SPIO, NLC-SPIO and Gal-NLC-SPIO/PEG, and the particle size of magnetic lipid nanoparticles was approximately 50 nm. The result was similar to that from zetasizer.

Preprints (www.preprints.org) | NOT PEER-REVIEWED | Posted: 24 July 2018 doi:10.20944/preprints201807.0459.v1

Peer-reviewed version available at Quant. Imaging Med. Surg. 2018, 8, 770-780; doi:10.21037/qims.2018.09.03

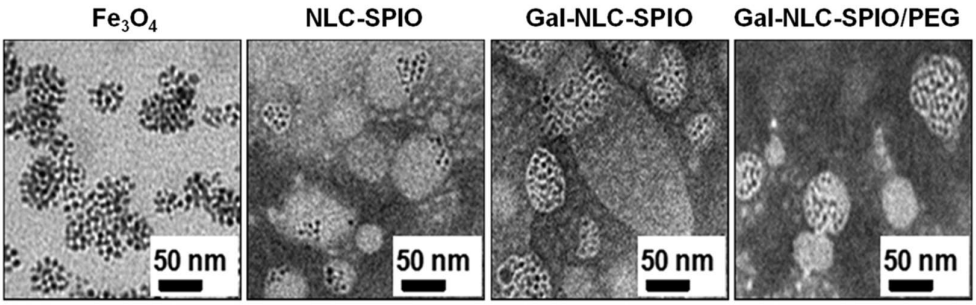

Figure 2. Preparation and characteristics. TEM images of Fe_3O_4, NLC-SPIO, Gal-NLC-SPIO and Gal-NLC-SPIO/PEG nanoparticles (× 100,000, bar = 50 nm).

As shown in Figure. S2, the MNLC was in aqueous solution at room temperature for > 1 month. MNLC could be precipitate using external magnetic field overnight and redispersed after the external magnetic field was removed. This type of precipitation-redispersion could be repeated many times, suggesting that the SPIO was successfully entrapped into MNLC, and the MNLC was very stable.

2.3 In vitro cytotoxicity assay of the MNLC

The cytotoxicities of Gal-NLC-SPIO, NLC-SPIO and Gal-NLC-SPIO/PEG were tested by MTT method and colorimetric cell viability assay. Using LO2, HepG2, and RAW264.7 cell lines as model tumor cells, the results in Figure S3 displayed that cell viability was still higher than 80% even when the concentration of Fe_3O_4 was reached up to 100 μg mL^{-1} (nanoparticles was 1 mg mL^{-1}), which indicated the MNLC had relatively low cytotoxicity and high biocompatibility for both tumor cells and normal cells.

2.4 Cellular internalization ability of the MNLC

In order to investigate the targeting ability of Gal-NLC-SPIO toward LO2 cells, cellular competitive uptake of RITC labeled MNLC on LO2/HepG2 cells co-cultured systems were observed by a confocal laser scanning microscopy in Figure 3b.

Obviously, Line 3 in Figure 3b indicated that there was significant difference in the cellular uptake of Gal-NLC-SPIO on the LO2/HepG2 cells co-cultured systems. The cellular uptake of Gal-NLC-SPIO on LO2 cells was more efficient compared with HepG2 cells co-cultured. However, NLC-SPIO and Gal-NLC-SPIO/PEG showed approximate uptake on the LO2/HepG2 cells co-cultured systems (Line 1 and 2 in Figure 3b).

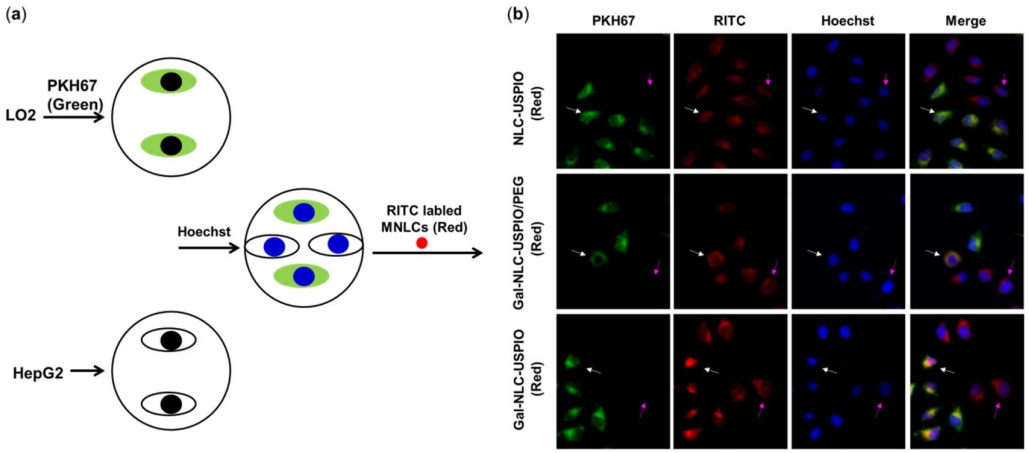

Peer-reviewed version available at Quant. Imaging Med. Surg. 2018, 8, 770-780; doi:10.21037/qims.2018.09.03

Figure3. Cellular competitive uptake studies. (a) Schematic diagram of cellular competitive uptake of Gal-NLC-SPIO, NLC-SPIO and Gal-NLC-SPIO/PEG. (b) Confocal microscopy images of RITC labeled MNLC for 1 h. LO2 cells (the cytoplasmic membrane labeled with PKH67 fluorescent linker, Green) co-cultured with HepG2 cells were incubated with RITC-Gal-NLC-SPIO, RITC-NLC-SPIO and RITC-Gal-NLC-SPIO/PEG (Red). The nucleus were all stained with Hoechst 33342. The white arrow stands for LO2 cells, the pink arrow stands for HepG2 cells.

The cellular competitive uptake data confirmed strong and specific binding of the Gal-NLC-SPIO to LO2 cells, due to the presence of an abundant ASGPR on the LO2 cell surface [26-28]. The results of qualitative and quantitative cellular uptake for FITC labeled Gal-NLC-SPIO, NLC-SPIO and Gal-NLC-SPIO/PEG were presented (Figure 4) after the MNLC were incubated with LO2, HepG2 and RAW264.7 cells for 1 h and 12 h, respectively. It was found that the SPIO could be internalized into cells mediated by the MNLC. And the uptake of the Gal-NLC-SPIO, NLC-SPIO and Gal-NLC-SPIO/PEG by LO2, HepG2 and RAW264.7 cells were time dependent. The SPIO accumulation in RAW264.7 cells by NLC-SPIO was faster than Gal-NLC-SPIO and Gal-NLC-SPIO/PEG. The SPIO accumulation in LO2 cells by Gal-NLC-SPIO was faster than NLC-SPIO and Gal-NLC-SPIO/PEG while there were no obvious difference among the magnetic NLCs in HepG2 cells. The cellular uptake data confirmed strong and specific targeting ability of the NLC-SPIO to RAW264.7 cells and Gal-NLC-SPIO to LO2 cells.

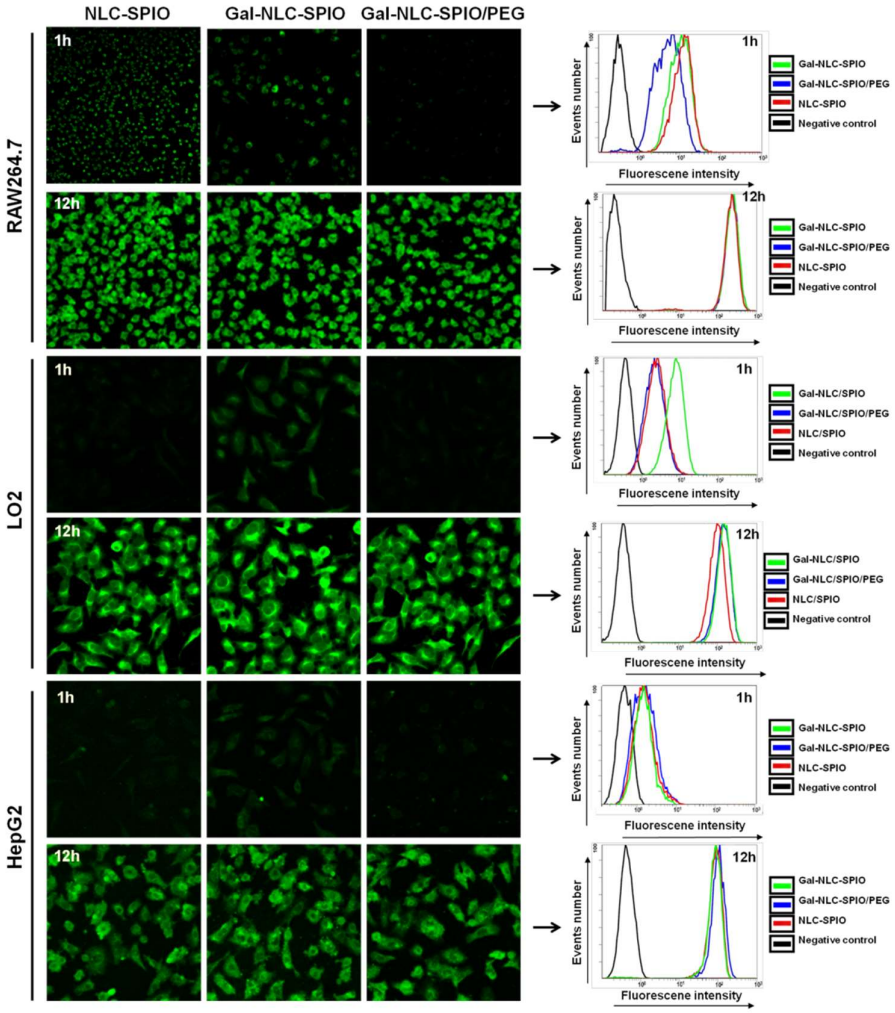

Figure 4. In vitro cellular uptake of MNLC in different cell lines. Fluorescence images observed by confocal microscopy and fluorescence intensity inside cells measured by flow cytometry of LO2,

Peer-reviewed version available at Quant. Imaging Med. Surg. 2018, 8, 770-780; doi:10.21037/qims.2018.09.03

HepG2 and RAW264.7 cells incubated with FITC-Gal-NLC-SPIO, FITC-NLC-SPIO and FITC-Gal-NLC-SPIO/PEG for 1 h and 12 h, respectively.

2.5 Liver distribution of MNLC in vivo

Liver distribution were important prerequisites for diagnosing of liver disease. To further investigate whether MNLC could targeting to liver *in vivo*, DiR was loaded in MNLC and used as fluorescence probe for in vivo imaging. After injection of DiR loaded MNLC, accumulation of DiR fluorescence in the liver was time dependent and the fluorescence intensity increased gradually, the fluorescence intensity of liver injected by Gal-NLC-SPIO/DiR was stronger than NLC-SPIO/DiR and Gal-NLC-SPIO/PEG/DiR as shown in Figure 5a. The results in Figure 5b also demonstrated that the fluorescent signal values of the Gal-NLC-SPIO to livers were significantly stronger than those of NLC-SPIO and Gal-NLC-SPIO/PEG in livers at every time points, suggesting that Gal-NLC-SPIO has specific target ability to liver and was expected to become MRI contrast agent.

2.6 In vitro MR imaging of MNLC

Magnetic properties were important parameters for an MRI contrast agent. As showed in Figure 5c, the T2-weighted MRI of Gal-NLC-SPIO at a 3.0 T clinical MRI instrument presented obvious color change with a variation of Fe_3O_4 concentration. It was found that Gal-NLC-SPIO exhibited negative contrast enhancement as the Fe_3O_4 concentration increased from 0 to 100 μg mL^{-1}. The relaxation rate, R2 = 1/T2, linearly proportional to the Fe concentration was also shown in Figure 5d. It was indicated that Gal-NLC-SPIO showed favorable contrast effect. The high relaxivity coefficient was prerequisite to be utilized as novel T2 negative contrast agent for sensitive MR imaging.

T2-weighted images of Gal-NLC-SPIO, NLC-SPIO and Gal-NLC-SPIO/PEG incubated with LO2 and HepG2 cells for 1 h and their intensity were showed in Figure 5e. The T2-weighted image intensity of blank cells were similar with that of water, while after the uptake of MNLC, the T2-weighted image intensity was significant declined. The T2-weighted image intensity of LO2 cells incubated with Gal-NLC-SPIO was decreased most prominent, which existed significant differences compared with others ($P < 0.01$). This may due to the specific binding activity of Gal-NLC-SPIO nanoparticles to LO2 cells leading to the over expression of receptor on the cell surface and the receptor-mediated endocytosis to enhance the tumor cells uptake [28].

Peer-reviewed version available at Quant. Imaging Med. Surg. 2018, 8, 770-780; doi:10.21037/qims.2018.09.03

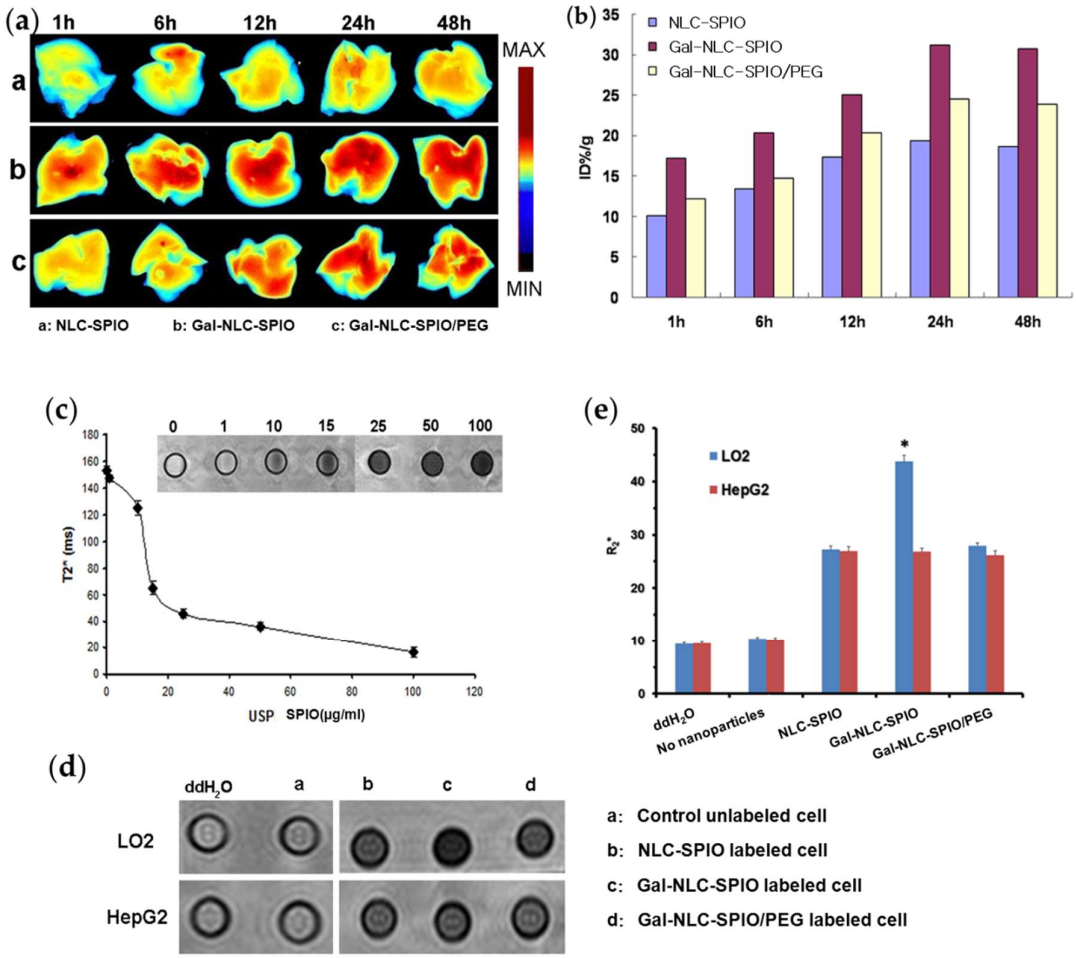

Figure 5. Bioimaging studies in orthotopic models. In vivo fluorescence imaging (a) and fluorescent semi-quantitative analysis (b) of normal nude mice liver after intravenous injection of DiR labled NLC-SPIO (a), Gal-NLC-SPIO (b) and Gal-NLC-SPIO/PEG (c) in different time. MR imaging of magnetic NLCs in vitro. (c) T2-weighted images of Gal-NLC-SPIO at different iron concentrations and the chart of $T2^*$ values of Gal-NLC-SPIO changing with iron concentrations. (d) LO2 cells or HepG2 cells were incubated with three different kinds of magnetic NLCs for 1 h, and then scanned with MRI. (e) $R2^*$ values of LO2 cells or HepG2 cells in different groups were measured (*$p<0.01$).

2.7 In vivo MR imaging of MNLC and pathology studies

Both in vitro cellular uptake and MR imaging studies indicated that Gal-NLC-SPIO nanoparticles could target LO2 cells. *In vivo* MR imaging of MNLC were then examined using orthotopic implantation hepatoma models. T2 images of nude mice bearing HepG2 orthotopic implantation tumor were obtained before contrast and after injection of Gal-NLC-SPIO, NLC-SPIO and Gal-NLC-SPIO/PEG (Figure 6a), and the contrast-to-noise ratio（CNR）of T2-weighted MR signal intensity of the tumors were shown in Figure 6b. The results showed that the liver images of post-injection of three MNLC for 0.5 h and 3 h become darkened significantly compared with that of pre-injection of MNLC, the SNR of T2-weighted images intensity of livers were significantly decreased ($P < 0.05$), while no obvious difference was observed in the SNR of the T2-weighted images intensity of tumors between pre-injection and post-injection of MNLC（$p>0.05$）. Thus, the CNR of the tumor-liver was significantly increased after the injection of the Gal-SLN-SPIO compare with those of NLC-SPIO and Gal-NLC-SPIO/PEG（$p<0.05$）, indicating that the Gal-SLN-SPIO enhanced the contrast in liver tissue and might be used as a T2 negative contrast agent for MR imaging application.

Peer-reviewed version available at Quant. Imaging Med. Surg. 2018, 8, 770-780; doi:10.21037/qims.2018.09.03

To further verify the accumulation of iron at tumor tissue, the tissue slices were stained with haematoxylin-eosin (H&E) and Prussian blue. As shown in Figure 6c-i, the tumor cells were larger, pleomorphic and had bigger nucleus, abundant cytoplasm, which confirmed that the orthotopic implantation hepatoma models were successfully established. The accumulation of iron could be much more detected in the liver tissues of Gal-NLC-SPIO injected group (Figure 6c-iii) than that of NLC-SPIO and Gal-NLC-SPIO/PEG injected groups (Figure 6c-ii, 6c-iv). These results indicated that Gal-NLC-SPIO could target to the liver tissue more efficiently and reduced toxicity. This was mainly because Gal-NLC-SPIO successfully inherited the specific target ability to liver cells LO2.

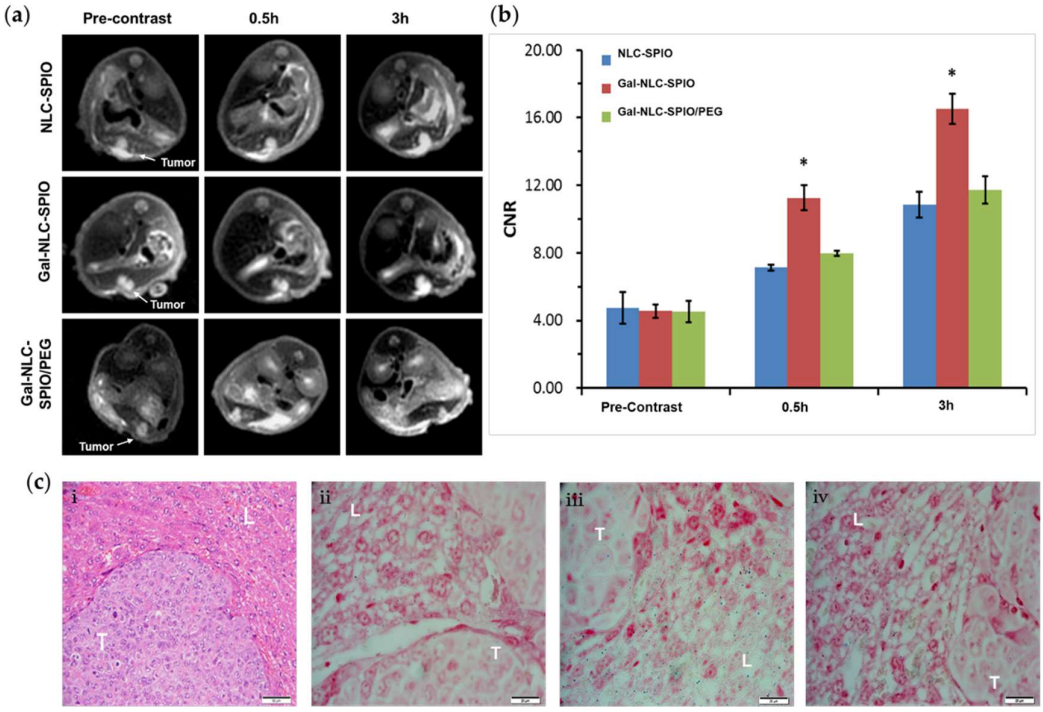

Figure 6. MR imaging and biodistribution studies. (a) T2-weighted single shot fast spin echo images of nude mice bearing HepG2 orthotopic implantation tumor before contrast and at 0.5 h and 3 h postinjection of three kinds of MNLC, respectively. The pink arrow stands for tumors. (b) Comparison of CNR of tumor-liver of the three group nude mice at different time point before and after contrast. (c) Microscopic view of HE stained tumor tissue section from nude mice bearing HepG2 tumor (i, magnification:×400); Prussian blue-stained tumor-liver tissue section of nude mice treated with NLC-SPIO (ii), Gal-NLC-SPIO (iii) and Gal-NLC-SPIO/PEG (iv), respectively. (ii, iii and iv, magnification: ×1000), "L" stands for the normal liver, "T" stands for the tumor.

3. Discussion

Asialoglycoprotein receptor (ASGPR) is a specific endocytotic receptor of mammalian hepatocytes, which has a predetermined selectivity for oligosaccharide or oligosaccharide protein of galactose residues from the end of the molecule in the circulation. Therefore, galactose-modified MNLCs can be applied as a hepatocyte-targeted nano-drug delivery system, which has significant clinical value for evaluation of liver disease. Here, it is important to determine if the delivery system is effective and safe. In this study, the novel liver-targeted MRI contrast agents Gal-NLC-SPIO had exhibited very low acute toxicity and reasonably good biocompatibility, it is suggested that SPIO loading does not affect the biosafety of the MNLCs (Figure S3). Moreover, the study also found that Gal-NLC-SPIO uptake by LO2 cells was significantly higher and easier than Gal-NLC-SPIO/PEG and free Gal in vitro due to the specific interaction between and ASGPR on hepatocytes. Interestingly, Gal-NLC-SPIO uptake by HepG2 cells is relatively rare (Figures 3-6), this can be attributed to (1) the narrow size distribution and biocompatible of Gal-NLC-SPIO (Figure 2), (2) the

Peer-reviewed version available at Quant. Imaging Med. Surg. 2018, 8, 770-780; doi:10.21037/qims.2018.09.03

targeted modification with galactose ligand, which enabled it to specifically internalize into LO2 cells and greatly enhance the hepatocyte targeting by EPR effect and selective binding of ASGPR (Figure 3). However, ASGPR expression of hepatocytes remained at a very low level in disease states, thus resulted in the relatively weak targeting capabilities of Gal-NLC-SPIO in HepG2 cells. Due to the significant difference of Gal-NLC-SPIO in cellular internalization and magnetic resonance imaging between LO2 and HepG2 cells, it is possible that Gal-NLC-SPIO is promising as a novel MRI contrast agent for diagnosis of liver disease.

4. Materials and Methods

4.1 Cell lines and culture conditions

RAW264.7 cells (mouse macrophage cell line), LO2 cells (human hepatic cell line) and HepG2 cells (human hepatocellular carcinoma cell line) were investigated in this study, and they are commercially available from Institute of Biochemistry and Cell Biology (Shanghai, China). RAW264.7, LO2 and HepG2 cells were maintained in Dulbecco's Modified Eagle's Medium (DMEM) at 37℃ in a humidified atmosphere containing 5% CO_2. All the mediums were supplemented with 10% (v/v) fetal bovine serum (FBS) and penicillin/streptomycin (100 U mL^{-1}, 100 U mL^{-1}). Cells were sub-cultured regularly using trypsin/ethylene diamine tetraacetic acid (EDTA).

4.2 Synthesis of Gal-ODA

The Gal-ODA conjugate was synthesized by the acylation between carboxyl group of LA derived from lactose and amino group of ODA. LA was coupled with ODA using 1-ethyl-3-(3-dimethyl aminopropyl) carbodiimide hydrochloride (EDC) as the coupling agent. Briefly, 1 g of LA, 0.5 g of ODA and 1.76 g of EDC were dissolved in 50 mL of ethanol solution in water bath at 60℃ for 24 h. After reaction, the reaction mixture was cooled to room temperature, and 50 mL of distilled water was then added to the mixture to precipitate the Gal-ODA. The precipitate was collected by filtration with 0.45 μm millipore filter and washed thrice by 50 mL distilled water. The final product was lyophilized, and the Gal-ODA was received.

4.3 Preparation of magnetic nanostructured lipid carriers (MNLC)

Galactose-conjugated MNLC (Gal-NLC-SPIO) was prepared using the solvent diffusion method. Briefly, 1 mL of Fe_3O_4 dispersion were added into 47 mL of 0.1% Poloxamer 188 in deionized water solution followed by sonication for 30 minutes using a probe sonicator (600 W, Sonicator JY92-II DN, Zhejiang, China) working 2 s following stopping 3 s to form a dispersion of magnetic nanoparticles. To stabilize the nanoparticles, 1 mL of oleic acid in ethanol solution (5 mg/mL) was added and sonicated for 5 minutes. Subsequently, 32 mg of monostearin and 3 mg of Gal-ODA were dissolved in 2 mL of ethanol solution at 70℃ and immediately injected into the aqueous dispersion of magnetic nanoparticles in an ultrasound waterbath at 70℃. The pre-emulsion was then cooled down to room temperature until magnetic nanoparticles of Gal-NLC-SPIO were obtained. As a control, NLC-SPIO and Gal-NLC-SPIO/PEG were prepared as described above.

4.4 Physicochemical characteristics of MNLC

^1H Nuclear magnetic resonance (NMR) spectra were used to analyze the synthesized Gal-ODA. LA, ODA and Gal-ODA were dissolved in D_2O at the concentration of 20 mg/mL, and measured using a NMR spectrometer (AC-80, Bruker Biospin, Germany). The particle size and zeta potential of the MNLC were measured by dynamic light scattering using a zetasizer (3000HS, Malvern Instruments Ltd, Worcestershire, UK). Morphological examination of the MNLC was performed using transmission electron microscopy (TEM, JEOL JEM-1230, Tokyo, Japan). The samples were stained with 2% (w/v) phosphotungstic acid and placed on copper grids with films for viewing.

4.5 Cytotoxicity assay in vitro

Peer-reviewed version available at Quant. Imaging Med. Surg. 2018, 8, 770-780; doi:10.21037/qims.2018.09.03

In order to investigate the cytotoxicity of MNLC, the methyl tetrazolium (MTT) assay was performed on the test cells according to the method described previously. Briefly, three kinds of cells were seeded in a 96-well culture plate (Nalge Nune Interational, Naperville, IL, USA), respectively, at a density of 10000 cells per well in 200 μL of complete medium. After cultured at 37°C for 24 h, the cells were exposed to a series of concentrations of magnetic nanoparticles for another 48 h. At the end of incubation, cells were incubated with 20 μL MTT solution (5 mg/mL) each well for further 4 h at 37°C. After that, 100 μL of dimethyl sulfoxide (DMSO) was added into each well to replace the culture medium and dissolve the insoluble formazan-containing crystals. Finally, the plates were shaken for 10 min, and optical density was measured at 570 nm using an automatic reader (Bio-Rad, Model 680, USA). Cell viability was calculated in reference to cells incubated with culture medium alone. All the experiments were repeated thrice.

4.6 Cellular uptake test of MNLC

To observe the cellular uptake, the fluorescein isothiocyanate (FITC) labeled MNLC were prepared using the conjugate of octadecylamine-fluorescein isothiocyanate (FITC-ODA). The FITC-ODA was synthesized by the reaction between amino group of ODA and isothiocyanate group of FITC as the previous report. The FITC labeled MNLC were prepared using 5 mg FITC-ODA instead of monostearin.

RAW264.7, LO2 and HepG2 cells were seeded onto 10 mm coverslips in a 24-well plate (Nalge Nunc International, Naperville, IL, USA), respectively, at a density of 50 000 cells per well in 1 mL of growth medium and allowed to attach for 24 h. Cells were then exposed to growth medium containing 50 μg/mL FITC labeled MNLC for further incubation. After that, 20 μL Hoechst (0.1 g/L) was added to stain the Cell nuclei for 30 min. Following the incubation, cells were then washed thrice with phosphate buffer saline (PBS) (pH 7.4) and, then, fixed with fresh 4% paraformaldehyde at 4°C for 20 min. The coverslips were observed under a confocal laser scanning microscope (LSM-510 META, ZEISS, Heidelberg, Germany). For the quantitative analysis of cellular uptake, cells were treated with trypsin after 24 h incubation with the three kinds of magnetic lipid nanoparticles, respectively, and then, re-suspended in PBS. The intensity of cellular fluorescence was evaluated by a flow-cytometer (FC500MCL, Beckman Coulter, Fullerton, CA, USA).

4.7 In vitro MR imaging of MNLC

A 3.0 T clinical MR scanner (GE, Discovery MR 750, USA) was used for in vitro MR imaging experiment. We determined the differences between the two kinds of nanoparticles-labeled cells in MR relaxation time. The two kinds of cells labeled with different kinds of MNLC were suspended in 0.5% agarose before being transferred into 1.5-ml microcentrifuge tubes (Eppendorf, Westbury, NY, USA). Each tube contained 1×10^5 cells. The tubes were imaged with an eight-channel phased-array head coil on the MR scanner.

4.8 In vivo MR imaging studies

Male BALB/C+nu/F1 nude mices were provided by the Zhejiang Medical Animal Centre were supplied with plenty of food and water. All animal experiments were conducted according to the National Institutes of Health (NIH, USA) guidelines for the care and use of laboratory animals. Meanwhile, all surgical procedures and experiment procedures were approved by the Committee for Animal Experiments of Zhejiang University.

About 2 weeks later, mice bearing HepG2 tumors of approximately 2 mm3 were randomized into 3 groups and taken for MR imaging equipped with a special coil designed for small animal imaging. T2-weighted MR images were acquired before MNLC (200 μL, 100 μg/mL) was injected via tail vein. Then the mice were imaged again at the predetermined time (0 h, 1 h, 3 h) after the injection.

Peer-reviewed version available at Quant. Imaging Med. Surg. 2018, 8, 770-780; doi:10.21037/qims.2018.09.03

4.9 Histological analysis

Animals were sacrificed to remove the liver for histological analysis. The tissues were fixed with 10% neutral buffered formalin and embedded in paraffin then sectioned. The sections were stained with haematoxylin-eosin (H&E) for histological analysis. Prussian blue staining was carried out to visualize accumulation of iron in the tissues. The microscopic images were photographed by a fluorescence microscopy (Leica, Germany).

4.10 Statistical analysis

The data were expressed as the mean of three separate experiments. The statistical significance of the differences between groups were assessed using the Student's t-test for each paired experiment, and a P value <0.05 was considered statistically significant in all cases.

5. Conclusions

In this study, Gal-ODA graft was designed and synthesized successfully via esterification reaction and could form MNLC in aqueous solution for the delivery of superparamagnetic iron oxide. The Gal-NLC-SPIO nanoparticles were effectively transported to the liver tissue through the EPR effect, the targeting peptide Gal enhanced endocytosis of the nanoparticles, then could achieve diagnostic and monitoring purposes. The assay of in vitro and in vivo activities indicated that Gal-NLC-SPIO has a better targeting ability to liver compared with NLC-SPIO and Gal-NLC-SPIO/PEG. The research suggests that, with the mediation of homing peptide Gal, the Gal-NLC-SPIO has the potential for liver-targeting molecular imaging. Therefore, Gal-NLC-SPIO is especially promising as liver-targeted molecular MRI contrast agent for further clinical utilization.

Supplementary Materials: Supplementary materials can be found at www.mdpi.com/xxx/s1.

Author Contributions: Conceptualization, Y.Z.D. and R.S.Y.; Methodology, X.L.Z. and C.Y.L.; Software, L.Y.; Validation, X.L.Z., Y.Z.D and R.S.Y.; Formal Analysis, C.Y.L. and Z.H.W.; Investigation, Q.Z. and W.L.; Resources, Y.Z.D. and R.S.Y.; Data Curation, Y.C. and L.Y.J.; Writing-Original Draft Preparation, X.L.Z. and Z.H.W.; Writing-Review & Editing, Y.Z.D. and R.S.Y.; Visualization, X.X.; Supervision, Y.Z.D. and R.S.Y.; Project Administration, R.S.Y.; Funding Acquisition, Y.Z.D., R.S.Y. and Z.H.W.

Funding: This research was funded by the Nature Science Foundation of Zhejiang province under Contract LY18H180003, and the National Natural Science Foundation of China under Contract 81571662, 81171334, and 81760643.

Acknowledgments: The authors acknowledge that the Institute of Pharmaceutics at Zhejiang University provided key laboratory facilities for this research.

Conflicts of Interest: The authors declare no conflict of interest.

Abbreviations

NLCs	Nanostructured lipid carriers
MRI	Magnetic resonance imaging
MNLCs	Magnetic nanostructured lipid carriers
ODA	Octadecylamine
Gal-ODA	Galactose-octadecylamine
LA	Lactose acid
SPIO	Superparamagnetic iron oxide
MR	Magnetic resonance
MRCAs	Magnetic resonance contrast agents
Gd	Gadolinium
Mn	Manganese
RES	Reticuloendothelial system
NLC	Nanostructured lipid carriers
ASGPR	Asialoglycoprotein receptor

Peer-reviewed version available at *Quant. Imaging Med. Surg.* **2018**, *8*, 770-780; doi:10.21037/qims.2018.09.03

Gal	Galactose
Gal-NLC	Galactose-conjugated nanostructured lipid carriers
FBS	Fetal bovine serum
DMEM	Dulbecco's modified eagle's medium
EDTA	Ethylene diamine tetraacetic acid
EDC	1-ethyl-3-(3-dimethyl aminopropyl) carbodiimide hydrochloride
NMR	Nuclear magnetic resonance
TEM	Transmission electron microscopy
MTT	Methyl tetrazolium
DMSO	Dimethyl sulfoxide
FITC	Fuorescein isothiocyanate
FITC-ODA	Octadecylamine-fluorescein isothiocyanate
PBS	Phosphate buffer saline
H&E	Haematoxylin-eosin
CNR	Contrast-to-noise ratio

References

1. Gong MF.; Yang H.; Zhang S.; Yang Y.; Zhang D.; Li ZH.; Zou lg. Targeting T1 and T2 dual modality enhanced magnetic resonance imaging of tumor vascular endothelial cells based on peptides-conjugated manganese ferrite nanomicelles. *Int J Nanomedicine* **2016**, 11, 4051-4063. DOI: 10.2147/IJN.S104686.
2. Terreno E.; Castelli DD.; Viale A.; Aime S. Challenges for molecular magnetic resonance imaging. *Chem Rev* **2010**, 110, 3019-3042. DOI: 10.1021/cr100025t.
3. Xie J.; Liu G.; Eden HS.; Ai H.; Chen XY. Surface-engineered magnetic nanoparticle platforms for cancer imaging and therapy. *Accounts Chem Res* **2011**, 44, 883-892. DOI: 10.1021/ar200044b.
4. Major JL.; Meade TJ. Bioresponsive, cell-Penetrating, and multimeric MR contrast agents. *Accounts Chem Res* **2009**, 42, 893-903. DOI: 10.1021/ar800245h.
5. Hasserodt J.; Kolanowski JL.; Touti F. Magnetogenesis in water induced by a chemical analyte. *Angew Chem Int Ed Engl* **2014**, 53, 60-73. DOI: 10.1002/anie.201305662.
6. Lu J.; Ma SL.; Sun JY.; Xia CC.; Liu C.; Wang ZY.; Zhao XN.; Gao FB.; Gong QY, Song B.; et al. Manganese ferrite nanoparticle micellar nanocomposites aivs MRI contrast agent for ler imaging. *Biomaterials* **2009**, 30, 2919-2928. DOI: 10.1016/j.biomaterials.2009.02.001.
7. Lee SH.; Kim BH.; Na HB.; Hyeon T. Paramagnetic inorganic nanoparticles as T1 MRI contrast agents. *Wiley Interdiscip Rev Nanomed Nanobiotechnol* **2014**, 196-209. DOI: 10.1002/wnan.1243.
8. Na HB.; Song IC.; Hyeon T.; Inorganic nanoparticles for MRI contrast agents. *Adv Mater* **2009**, 21, 2133-148. DOI: 10.1002/adma.200802366.
9. Wu W.; Wu ZH.; Yu TY.; Jiang CZ.; Kim WS. Recent progress on magnetic iron oxide nanoparticles: synthesis, surface functional strategies and biomedical applications. *Sci Technol Adv Mater* **2015**, 16, 023501. DOI: 10.1088/1468-6996/16/2/023501.
10. Ghazani AA.; Pectasides M.; Sharma A.; Castro CM.; Mino-Kenudson M.; Lee H.; Shepard JA.; Weissleder R. Molecular characterization of scant lung tumor cells using iron-oxide nanoparticles and micro-nuclear magnetic resonance. *Nanomedicine* **2014**, 10, 661-668. DOI: 10.1016/j.nano.2013.10.008.
11. Li JC.; He Y.; Sun WJ.; Luo Y.; Cai HD.; Pan YQ.; Shen MW.; Xia JD.; Shi XY. Hyaluronic acid-modified hydrothermally synthesized iron oxide nanoparticles for targeted tumor MR imaging. *Biomaterials* **2014**, 35, 3666-3677. DOI: 10.1016/j.biomaterials.2014.01.011.
12. De Jong WH.; Borm PJ. Drug delivery and nanoparticles: applications and hazards. *Int J Nanomedicine* **2008**, 3, 133-149. PMID: 18686775.
13. Binnemars-Postma K.; Storm G.; Prakash J. Nanomedicine Strategies to Target Tumor-Associated Macrophages. *Int J Mol Sci* **2017**, 18, E979. DOI: 10.3390/ijms18050979.
14. Ngambenjawong C.; Cieslewicz M.; Schellinger JG.; Pun SH. Synthesis and evaluation of multivalent M2pep peptides for targeting alternatively activated M2 macrophages. *J Control Release* **2016**, 224, 103-111. DOI: 10.1016/j.jconrel.2015.12.057.
15. Du YZ.; Cai LL.; Liu P.; You J.; Yuan H.; Hu FQ. Tumor cells-specific targeting delivery achieved by A54 peptide functionalized polymeric micelles. *Biomaterials* **2012**, 33, 8858-8867. DOI: 10.1016/j.biomaterials.2012.08.043.

16. Chaudhary S.; Garg T.; Murthy RSR.; Goyal GAK. Development, optimization and evaluation of long chain nanolipid carrier for hepatic delivery of silymarin through lymphatic transport pathway. *Int J Pharm* **2015**, 485, 108–121. DOI: 10.1016/j.ijpharm.2015.02.070.
17. Situ JQ.; Wang XJ.; Zhu XL.; Xu XL.; Kang XQ.; Hu JB.; Lu CY.; Ying XY.; Yu RS.; You J.; Du YZ. Multifunctional SPIO/DOX-loaded A54 Homing Peptide Functionalized Dextran-g-PLGA Micelles for Tumor Therapy and MR Imaging. *Sci Rep* **2016**, 6, 35910. DOI: 10.1038/srep35910.
18. Shidhaye SS.; Vaidya R.; Sutar S.; Patwardhan A.; Kadam VJ. Solid lipid nanoparticles and nanostructured lipid carriers--innovative generations of solid lipid carriers. *Curr Drug Deliv* **2008**, 5, 324-331. DOI: 10.1070/QE1999v029n08ABEH001565.
19. Yingchoncharoen P.; Kalinowski DS.; Richardson DR. Lipid-Based Drug Delivery Systems in Cancer Therapy: What Is Available and What Is Yet to Come. *Pharmacol Rev* **2016**, 68, 701-787. DOI: 10.1124/pr.115.012070.
20. Beloqui A.; Solinis MA.; Rodriguez-Gascon A.; Almeida AJ.; Preat V. Nanostructured lipid carriers: Promising drug delivery systems for future clinics. *Nanomedicine* 2016, 12, 143-161. DOI: 10.1016/j.nano.2015.09.004.
21. Khan S.; Baboota S.; Ali J.; Khan S.; Narang RS.; Narang JK. Nanostructured lipid carriers: an emerging platform for improving oral bioavailability of lipophilic drugs. *Int J Pharm Investig* **2015**, 5, 182-191. DOI: 10.4103/2230-973X.167661.
22. Iqbal MA.; Md S.; Sahni JK.; Baboota S.; Dang S.; Ali J. Nanostructured lipid carriers system: recent advances in drug delivery. *J Drug Target* **2012**, 20, 813-830. DOI: 10.3109/1061186X.2012.716845.
23. Lu W.; He LC.; Wang CH.; Li YH.; Zhang SQ. The use of solid lipid nanoparticles to target a lipophilic molecule to the liver after intravenous administration to mice. *Int J Biol Macromol* **2008**, 43, 320-324. DOI: 10.1016/j.ijbiomac.2008.06.006.
24. Maeda H.; Nakamura H.; Fang J. The EPR effect for macromolecular drug delivery to solid tumors: Improvement of tumor uptake, lowering of systemic toxicity, and distinct tumor imaging in vivo. *Adv Drug Deliv Rev* **2013**, 65, 71-79. DOI: 10.1016/j.addr.2012.10.002.
25. Lee CM.; Jeong HJ.; Kim SL.; Kim EM.; Kim DW.; Lim ST.; Jang KY.; Jeong YY.; Nah JW.; Sohn MH. SPION-loaded chitosan-linoleic acid nanoparticles to target hepatocytes. *Int J Pharm* **2009**, 371, 163-169. DOI: 10.1016/j.ijpharm.2008.12.021.
26. Wang WY.; Zhao XL.; Hu HY.; Chen DW.; Gu JC.; Deng YH.; Sun J. Galactosylated solid lipid nanoparticles with cucurbitacin B improves the liver targetability. *Drug delivery* **2010**, 17, 114-122. DOI: 10.3109/10717540903580176.
27. Craparo EF.; Sardo C.; Serio R.; Zizzo MG.; Bondi ML; Giammona GG. Galactosylated polymeric carriers for liver targeting of sorafenib. *Int J Pharm* **2014**, 466, 172-180. DOI: 10.1016/j.ijpharm.2014.02.047.
28. Lian J.; Zhang S.; Wang J.; Fang K.; Zhang Y.; Hao Y. Novel galactosylated SLN for hepatocyte-selective targeting of floxuridinyl diacetate. *J Drug Target* **2008**, 16, 250-256. DOI: 10.1080/10611860801902351.